



HAL
open science

Determination of current density distribution in proton exchange membrane fuel cells

D. Candusso, J. Poirot-Crouvezier, B. Bador, E. Rullière, R. Soulier, J. Y. Voyant

► **To cite this version:**

D. Candusso, J. Poirot-Crouvezier, B. Bador, E. Rullière, R. Soulier, et al.. Determination of current density distribution in proton exchange membrane fuel cells. *European Physical Journal: Applied Physics*, 2003, 25, pp.67-74. 10.1051/epjap:2003079 . hal-04512963

HAL Id: hal-04512963

<https://hal.science/hal-04512963v1>

Submitted on 20 Mar 2024

HAL is a multi-disciplinary open access archive for the deposit and dissemination of scientific research documents, whether they are published or not. The documents may come from teaching and research institutions in France or abroad, or from public or private research centers.

L'archive ouverte pluridisciplinaire **HAL**, est destinée au dépôt et à la diffusion de documents scientifiques de niveau recherche, publiés ou non, émanant des établissements d'enseignement et de recherche français ou étrangers, des laboratoires publics ou privés.

Determination of current density distribution in Proton Exchange Membrane Fuel Cells

D. Candusso^a - J.P. Poirot-Crouvezier^b - B. Bador^c - E. Rullière^a - R. Soulier^a - J.Y. Voyant^a

^a Laboratoire d'Electrotechnique de Grenoble
UMR 5529 INPG/UJF - CNRS
ENSIEG - BP 46
38402 Saint-Martin-d'Hères Cedex - France
Rulliere@leg.ensieg.inpg.fr
Tel : (33) 4 76 82 62 94

^b LHPAC – CEA Grenoble
^c SETEX – CEA Grenoble
CEA Grenoble
17 rue des Martyrs
38054 Grenoble Cedex 9 - France
Baurens@cea.fr

Abstract. This study is to look at the distribution of current densities in Proton Exchange Membrane Fuel Cells (PEMFC) to enable optimisation of fuel cell performance. The feasibility of using a new measurement technique of the local magnetic field, in the conductive plates of the cell was studied. The magnetic field is measured throughout the cell using the Maxwell equations and the current densities calculated. The measurement system and its validation are outlined in the first section. The next section outlines the experimental current density distribution within the cell, operating under standard conditions and special configurations, such as the partially active Membrane Electrodes Assembly (MEA). Using a Matlab or Femlab model of the cell, (which is briefly outlined) our experiments are compared and an attempt made to explain the distribution of the current densities. Finally recent developments of the device are described, which will be used in several tests of PEMFC small stacks.

PACS. 84.60.Dn Electrochemical conversion and storage: electrochemical cells and batteries; fuel cells
89.20.Bb Industrial and technological research and development
41.20.Gz Magnetostatics; magnetic shielding, magnetic induction, boundary-value problems

1 Introduction

PEMFC are accepted as one of the best technologies, meeting the requirements for in-car applications with potentially major possibilities for them in portable and stationary systems due to their high power density and adaptability [1]. They are preferred to other Fuel Cells (FC) such as phosphoric acid or alkaline ones for many applications, because of their low operating temperature and solid electrolyte [2].

However they are still quite expensive devices, that is why it is very important to be able to improve the operating of the active MEA fuel cell area.

Temperature measurements at different places in the electrodes tend to show that the current distributions may be non-homogeneous especially in large cells [3,4]. This requires very careful study in order to be able to understand the causes and then optimise the operating of the cell.

Some techniques for determining the current density distribution have already been described [5]. One of these allows the placement of several electrically isolated subcells at suitably chosen locations within the MEA, each one being controlled by a separate load; the current-voltage characteristics for the subcells, when compared to those of the whole cell, are indicative of localised electrochemical activity in the fuel cell. A second method is the current distribution mapping [6] involving the use of a passive resistor network distributed throughout the MEA. A third method [7] uses Hall-effect current sensors with magnetic cores inserted in the collector plate for each subcell. These are very interesting techniques: the whole electrode area is thoroughly covered and time dependant phenomena can be monitored in real time. However the following limitations should be noted, the measurement device has an effect on the current distribution and it is a complex device.

Consequently an indirect evaluation of the current densities by measuring the locally induced magnetic field was preferred, as described in the next section [8].

2 Theoretical method and experimental technique used to evaluate the current density by measuring the electromagnetic field

2.1 Method and experimental device

Figure 1 shows the general structure of an elementary PEM cell. Several cells such as this one are generally assembled in order to provide sufficient voltage.

The electrodes are made of carbon material in which platinum grains are inserted to catalyse the electrochemical reactions. The Proton Exchange Membrane is a polymer fabric (Nafion), which allows proton transfer and creates a physical separation between the anode and the cathode.

The MEA is inserted between two conductive plates, which also provide gases (O₂ or H₂) to the electrodes and drain off the water. The cell is tested under the following standard conditions applied to all the experiments:

- H₂ and O₂ provided are pure and quite dry.
- The stoichiometric factors are fixed at 2 for both sides.
- The cell is not heated by an external device, it only heats itself. The temperature can be regulated by means of two fans.

The electric plugs of the experimental cell (current collectors) are situated on each side of the plates (Figure 1).

Using the Maxwell equations, the current density vector in the plate is related to the flux density:

$$\vec{J} = \frac{1}{\mu_0} \text{rot } \vec{B} \quad (1)$$

Using the notations of Figure 2 in which the MEA is located in the (\vec{x}, \vec{y}) plan, we get:

$$J_x = \frac{1}{\mu_0} \left(\frac{\partial B_z}{\partial y} - \frac{\partial B_y}{\partial z} \right) \quad (2)$$

$$J_y = \frac{I}{\mu_0} \left(\frac{\partial B_x}{\partial z} - \frac{\partial B_z}{\partial x} \right) \quad (3)$$

$$J_z = \frac{I}{\mu_0} \left(\frac{\partial B_y}{\partial x} - \frac{\partial B_x}{\partial y} \right) \quad (4)$$

Note that the collector plates are made of stainless steel grade 316, which was chosen for its excellent corrosion resistance. Its permeability is reputed to virtually equal the air permeability (μ_0) which is used in the above equations.

To compute the current densities on the MEA surface, the electromagnetic field should be measured as close to the MEA as possible. In order to show the feasibility of the method, we used an available FC which is a monocellular one with a 200 cm² active MEA. In this case, the J_x and J_y currents should be considered as well as J_z . But if the measurement is done far enough away from the current collectors plugs, then the contribution of J_x and J_y are small compared to J_z , so that only B_x and B_y will have to be measured.

In each conductive plate, there are four measurement borings (diameter is 6.5mm) every 30mm at a distance of 15mm (along \vec{z} axis) from the MEA surface. It is described in Figure 1 and 2.

In order to choose the right magnetic sensor, we evaluated the maximum possible field: 900 μ T, knowing the dimensions of the MEA area (140mm \times 140mm) as well as the maximum current (400A). We also had to consider the dimensions of the sensor, as it had to be placed into a pipe able to slide into the borings.

The Hall effect sensors are not suitable because they are mainly used for measuring higher magnetic fields (up to 1T) and are quite expensive. We chose a magnetoresistive sensor (from Philips - ref. KMZ 10C) with a max operating range of 9.42mT (ten times requirements) and which is compatible with the geometric constraints. Thermal probes have to be added, as the magnetic sensor output changes with temperature.

2.2 Measurement validation

At first, we studied the influence of added (\vec{x}) and (\vec{y}) borings on the magnetic field distribution. We also compared the sensor positioning to a grid/network of holes along \vec{z} axis using the Flux 2D software [9]. As J_z only is supposed to be computed, B_x (y) and B_y (x) are the useful components of the magnetic field, that is the reason why we used a 2D simulator.

The simulations give similar results for the different configurations. The second solution will give discrete values instead of continuous measurements along \vec{x} or \vec{y} axis and will lead to less accurate results on the current density distribution. The first experimental device has got (\vec{x}) borings only (Figure 3).

Also the temperature drift of the sensor was measured by a test bench with Helmholtz coils; it was ensured that there was no drift versus time. Using this pre-characterisation, the temperature correction is done after measurement using the twin values of field and thermal sensors.

The right dimensioning of the magnetoresistive sensor was validated by showing a linear relation between its output voltage (image of the magnetic field) and the current density on the range: 0-2A/cm² on the 200 cm² cell.

Finally, the experimental curve was compared (Figure 4): magnetic field B against x in the boring n°1 (situated on Figure 2) to the one computed by Flux 2D (Figure 5). The general parabolic shapes are similar but the experimental curve shows field peaks of a fairly large

amplitude. We studied the reasons for these peaks and had to set aside the influence of exterior magnetic fields. The "martensitic/austenitic" layer is more likely to induce these disturbances, which appears on the surface of the borings because of local drilling constraints.

To be free from these disturbances, we first thought of demagnetising the Fuel Cell plates; but we were not sure this would remain, as one should be able to determine the current distribution in any kind of FC made of magnetic or amagnetic material.

For this reason the measurements were taken of the magnetic field for a null current as well as the operating one. By subtracting the residual field for a null current, one can get the magnetic field due to the current flowing through the FC. Figure 6 and 7 show the curves of the field component B_x against x and the field component B_y against x after measurement and subtraction of the residual field. They have to be compared to figure 5 and 8 within the range $40 \leq x \leq 170\text{mm}$ where the curves have been computed using the Flux 2D simulator. The shapes are similar but the values of the field are different: the current density is $1\text{A}/\text{cm}^2$ for the simulated results whereas for the experiment, it varies with the placement. This mismatch is mainly due to deviations of currents towards collector plugs in our cell configuration, as shown in the next part of this paper, but is not derived from the field measurement process. A 3D simulation of the magnetic field would be more appropriate to match the experimental results, but as we said, our aim is to validate the method and then use a proper experimental device : a multi-stack Fuel Cell. FLUX 3D simulations are much longer and more complex than FLUX 2D ones.

As stated, only J_z is calculated, B_x and B_y are measured. The induction $B_x(y)$ is measured along each boring, which are equally spaced at every 30mm in the \bar{y} -axis direction. This allows us to determine $\partial B_x / \partial y$ for only 3 values of y , this will be sufficient for an overview of the current distribution in the cell all the more since B_x is theoretically supposed to be a linear function of y . $B_y(x)$ is measured every 15mm in the boring and the curve is then interpolated thanks to spline method under Matlab. These computations give the current density in the z -axis direction over an area covering approximately one third of the active area of the cell split into 42 elements (14×3).

The reproducibility of the current density evaluation method was validated as we got the same densities on each side of the FC (O_2 and H_2 side).

The next section details the experimental results when compared to a finite element model computing the local orientation of the current density distribution using FEMLAB software [10].

2.3 Experimental results

2.3.1 Case of a standard MEA

Figure 9 illustrates the results obtained for the current density distribution over the cell operating at 200 A, against x and y . For $x \geq 150$ mm, the current density decreases as there are no more channels (except those ones being placed for $37.5 \leq x \leq 177.5$ mm); the decrease is slow as some of the current dissipates beyond the active MEA area in search of a better conduction surface with less resistance. The derived value of the density (around $0.25 \text{ A}/\text{cm}^2$) is lower than $1 \text{ A}/\text{cm}^2$ average current density across the MEA; as we only measure J_z and not right at the MEA level. A simulation shows that the \bar{z} -axis density varies depending how far one is placed from the active part of the MEA. Figure 10 clearly shows the concurrent decrease of \bar{z} -axis density against x . This density increases as the direction of current points towards the collector plug.

The values of normal current density calculated with magnetic measurements are slightly different from the results of the simulation, the distribution of the current is similar, but the measured value is approximately half that of the calculated one. This discrepancy is partly due to the strong variations of the current direction and module near the borings and mainly to the side placement of the current collectors.

On Figure 9, a higher value of the density is found at the bottom of the cell than at the top of it. This can be explained by a non-homogeneous distribution of the current density over the active area: local conditions are better at the bottom of the cell than at the top. The electrolyte membrane may become more humidified at the bottom, because the gases introduced at the top are dry. Moreover, the bottom is warmer than the top. Thus, if the voltage is uniform over the cell, the current density is higher at the bottom.

This hypothesis was confirmed by the temperature measurements at the top and the bottom of the cell (Figure 11). Higher temperatures indicate that more heat is produced at the bottom of the cell. In a fuel cell, heat production is proportional to current production, so we can conclude that more current is produced at the bottom of this cell, as deduced from magnetic measurements.

2.3.2 Case of a Partial "catalysation" of the MEA

The initial experiments described above show that the technique is suitable for current density measurements over the area of a fuel cell. Even though current measurements have been confirmed by temperature measurements, it seemed advisable to conduct additional tests. In these tests, we demonstrated current distribution over the active area.

A specific MEA was assembled, with an active area of $70 \times 70 \text{ mm}^2$ which is one quarter of the total area. Tests were laid on for 30, 50 and 70A. The active part was successively placed at the bottom of the cell, then at the top of it, on the same and on opposite sides to the current collector plugs.

Figure 12 shows the experimental result for an operating current of 50A, which agrees with the placement of the active area at the top of the cell on the opposite side to the current collector plugs.

From the simulation, we got additional information concerning the current density distribution (Figure 13 and 14). Figure 13 shows the direction of the current density vector in the x-z plan; it confirms that the normal current density decreases rapidly outside the active area along the axis $z = 15 \text{ mm}$ (boring location). It only increases marginally in the current collector area. Taking into account the deviation of the current over the non-active area (Figure 14), it would seem that the normal current density is generally very low (practically zero) over the cell area, except over the active part, as measured.

3 Conclusion

The purpose of this study was to develop and validate an experimental device, which allows the current density distribution in a FC to be determined by measurement of the induced magnetic field.

Our findings have been interesting when compared to simulations using Flux 2D simulator and a Matlab – FEMLAB model.

In the type of FC studied there is a non-homogeneous current density distribution which is not the most efficient. Improvements can be made to the design of the cell so that the electrochemical activity is the same throughout the cell.

This work was undertaken on a mono-cell, where the current density vector direction varies considerably. It would be better to use a FC stack where the current density vector has a constant direction provided one is located far enough from the outside of the FC.

Enhanced measurement accuracy could be achieved by using both horizontal (\vec{x}) and vertical (\vec{y}) borings, which may slightly change the field map but will improve numerical differentiations. For J_x and J_y current density components, the measurement of induced field in the \vec{z} -axis direction would not be a significant advance, as its variations against x and y are consequent, as already shown by the case of a mono-cellular fuel cell. Also, the numerical differentiation of induction needs measurements at different z -coordinates, requiring to drill the collector plate like a grid. To avoid J_x and J_y currents would mean measuring fields in a bipolar and intermediate plate of a multi-stack fuel cell where currents are more likely to be uniformly orientated.

Our experimental device could be improved by utilising a two-axis magnetic sensor such as Honeywell HMC 1022S sensor.

This system could be used to demonstrate special techniques such as non-optimal "humidification" of the membrane (dryness), which may enable understanding of the non-homogeneity of the current density distribution.

The low price of magneto-resistive sensors would allow a permanent implantation within the fuel cells enabling the pressure and water contents of instantaneous injected gas to be regulated yielding improved performance.

The device developed here will soon be used within a small FC stack with a bipolar plate, where horizontal (\vec{x}) and vertical (\vec{y}) borings are made. The distribution of the current density over the whole active area will be obtained, due to the additional borings placed outside the active area.

1. L. Gerbaux, Modélisation d'une pile à combustible de type hydrogène/air et validation expérimentale, Ph.D. thesis, Institut National Polytechnique de Grenoble, 1996
2. L. J. M. J. Blomen, M. N. Mugerwa, *Fuel Cell Systems*, (Plenum Press, 1993).
3. J. P. Poirot-Crouvezier, D. Levrard, P. Baurens, Modélisation dynamique d'une pile De Nora destinée au véhicule électrique, in *Proceedings of the Millénaire de l'hydrogène – 10^{ème} conférence canadienne sur l'hydrogène*, Québec, 2000.
4. G. Maggio, V. Recupero, C. Montegazza, Modelling of temperature distribution in a solid polymer fuel cell stack, *Journal of Power Sources*, Vol. 62, pp. 167-174 (1996).
5. M. Nopponen, T. Mennola, M. Mikkola, T. Hottinen, P. Lund, Measurement of Current Distribution in a Free Breathing PEMFC, *Journal of Power Sources*, Proceedings of the 7th Grove Fuel Cell Symposium, Vol. 106(1-2), pp. 313-322, 2002.
6. Jürgen Stumper, Stephen A. Campbell, David P. Wilkinson, Mark C. Johnson, Mike Davis, In-situ methods for the determination of current distributions in PEM fuel cells, *Electrochimica Acta*. Vol 43, No. 24, pp. 3773-3783 (1998).
7. Measurement of current density and temperature distribution in polymer electrolyte fuel cells (PEFC), Institut für technische Thermodynamik, DLR (2000).
8. R. Soulier, Cartographie des densités de courant dans une pile à combustible par mesure du champ magnétique induit, Rapport de DEA de l'Institut National Polytechnique de Grenoble, 2001.
9. Flux 2D version 7.50, User's guide (Cedrat 2000)
www.cedrat.com/software/software.htm
10. <http://www.femlab.com/>

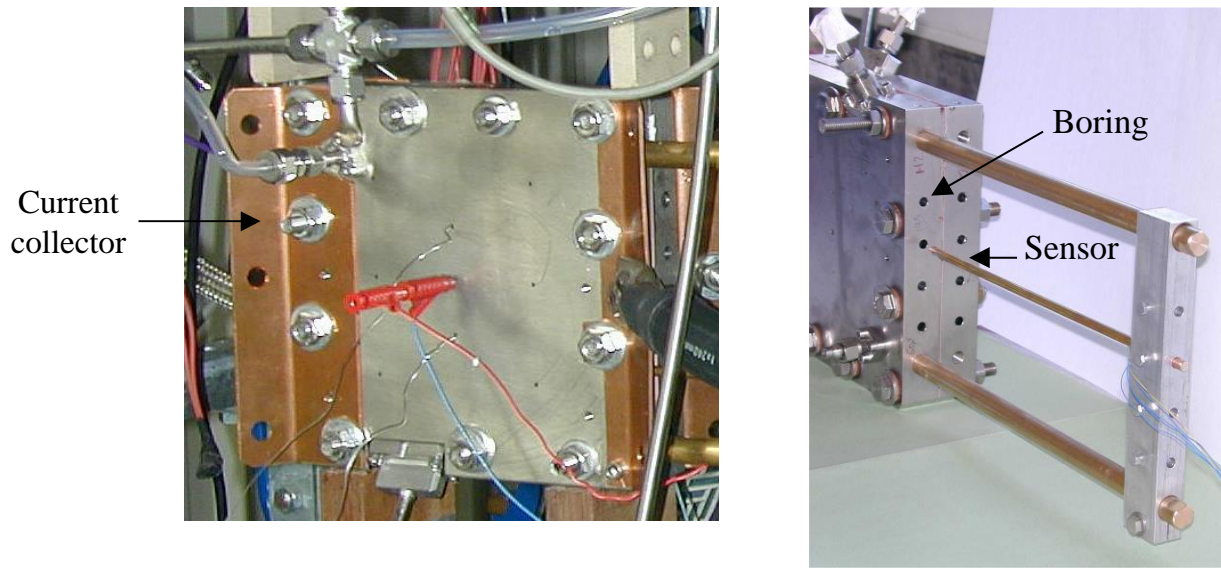


Fig. 1. The experimental device allowing the sensor to be inserted into the borings.

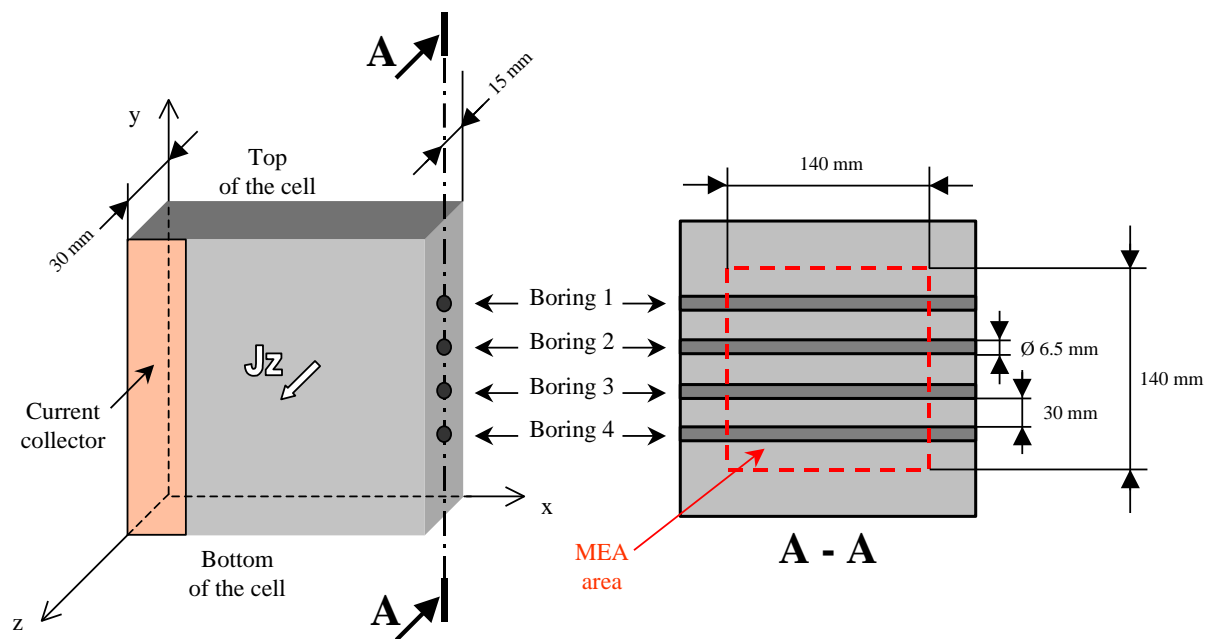


Fig. 2. Geometrical structure of the mono-cell.

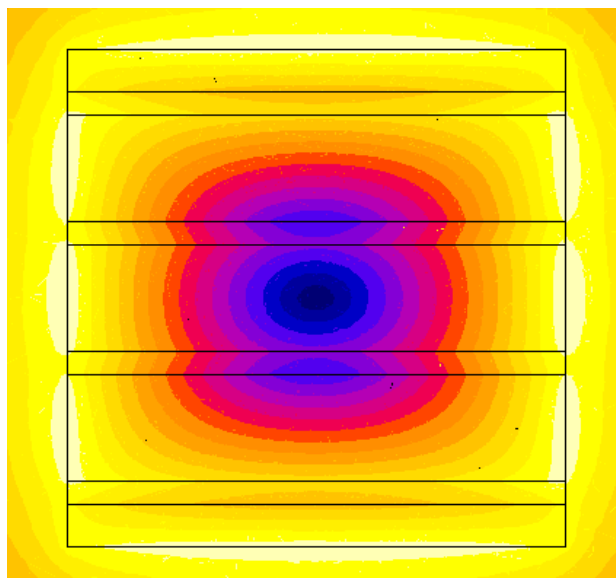


Fig. 3. Magnetic field distribution for the active area of the cell with \bar{x} borings only, according to FLUX 2D simulation. $J= 1A/ cm^2$

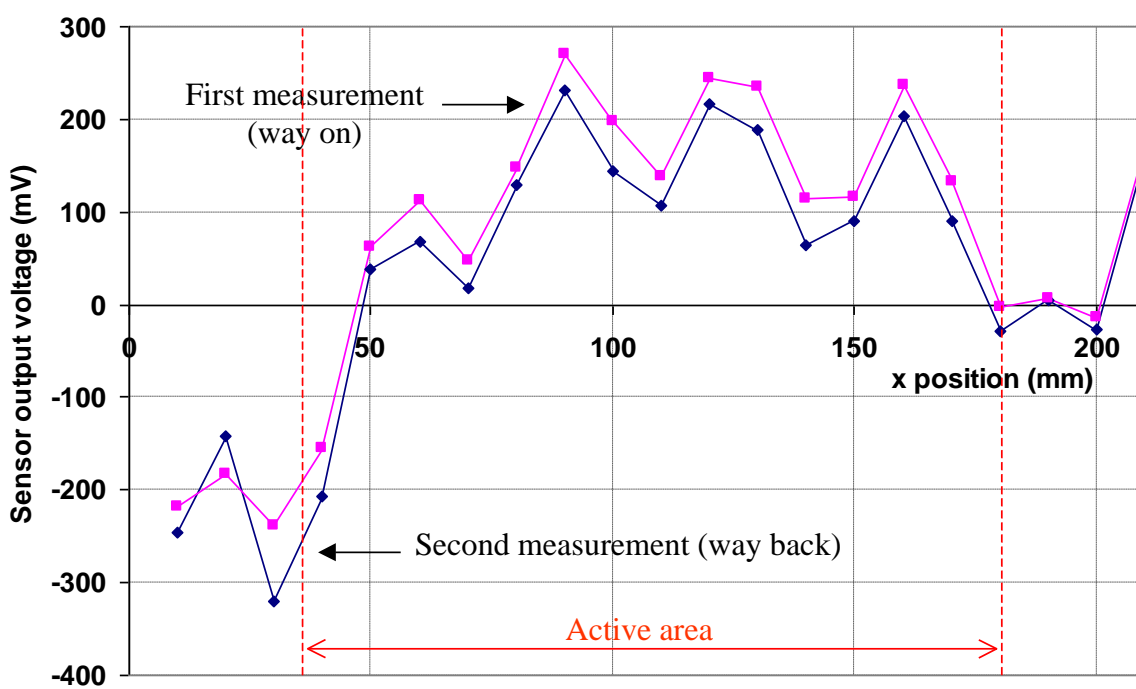


Fig. 4. Sensor output voltage versus x when inserted in the lower boring on the cathode side.

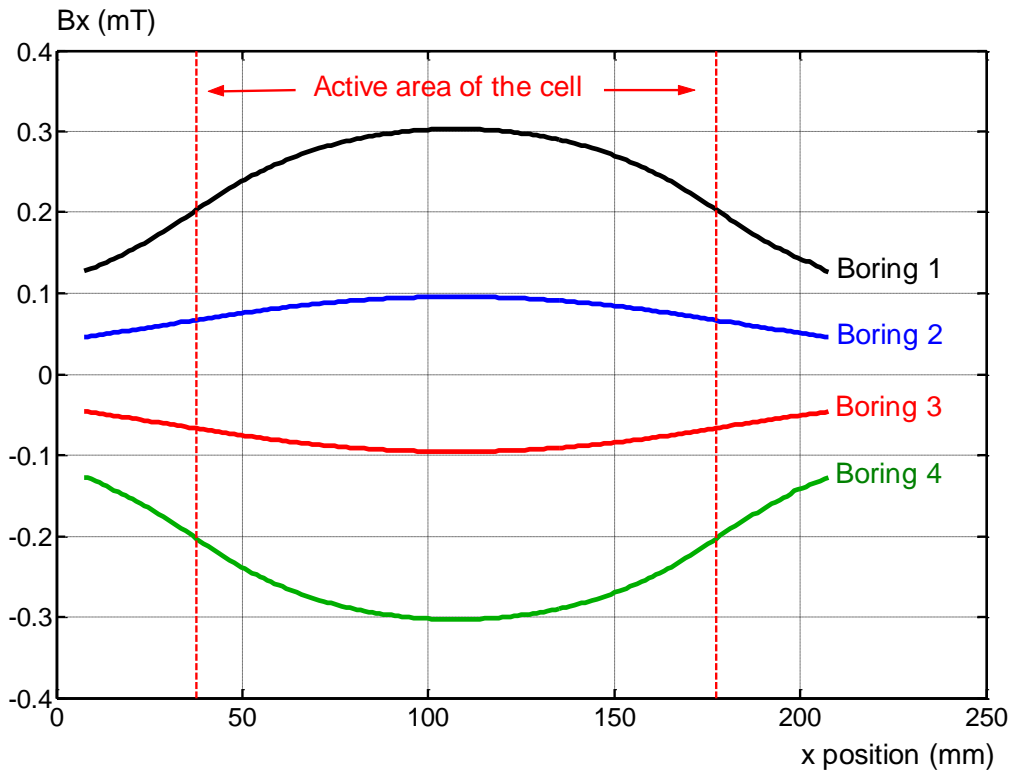


Fig. 5. FLUX 2D computed longitudinal magnetic field (B_x) versus x in the four borings ($j = 1\text{A}/\text{cm}^2$) at $z = 0$ (membrane).

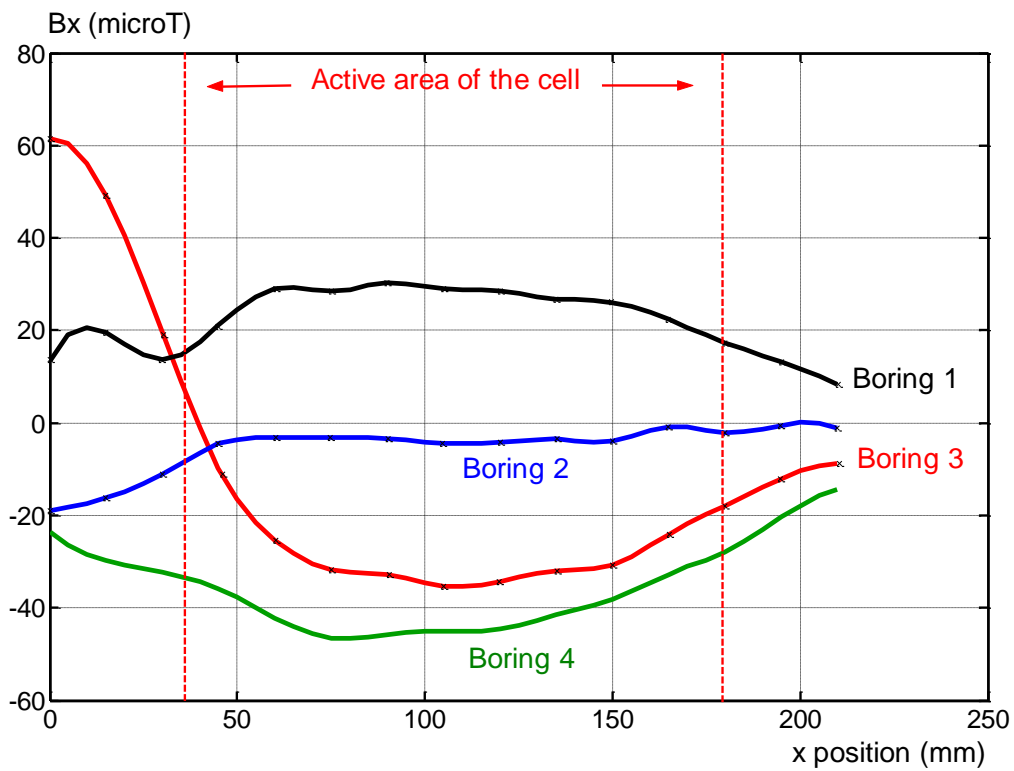


Fig. 6. Experimental longitudinal magnetic field (B_x) versus x after subtraction of the remnant field ($I = 0\text{A}$) when operating at $I = 200\text{A}$ (at $z = 15\text{mm}$).

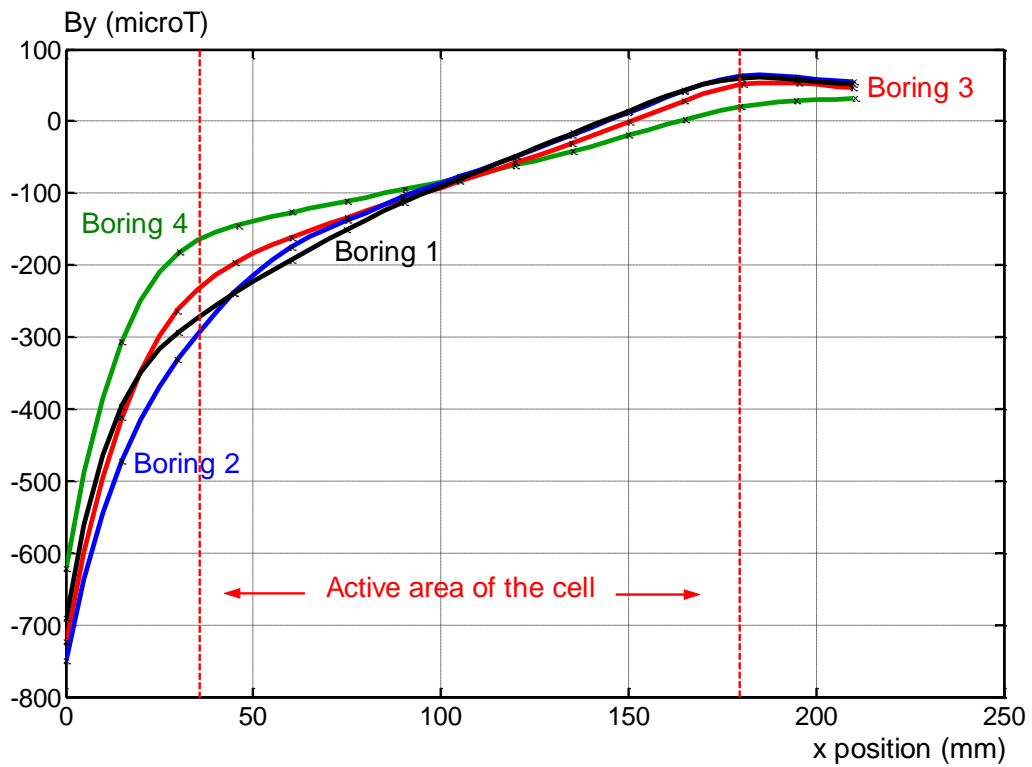


Fig. 7. Experimental vertical magnetic field (B_y) versus x after subtraction of the remnant field ($I = 0A$) when operating at $I = 200A$.

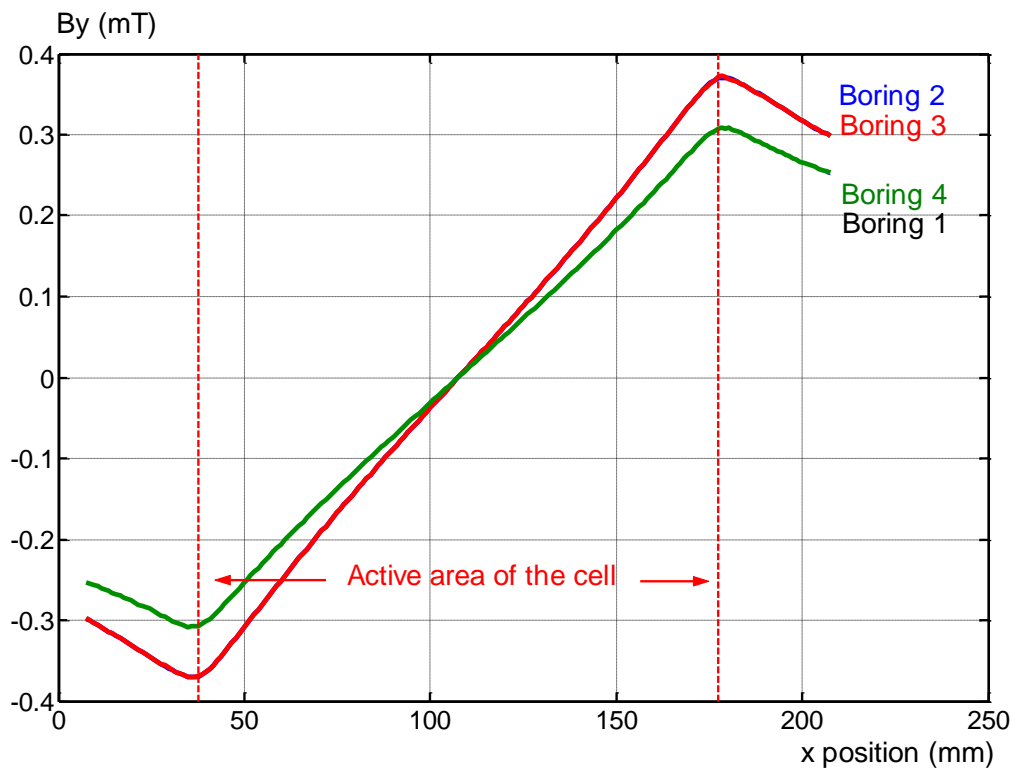


Fig. 8. FLUX 2D computed vertical magnetic field (B_y) versus x after subtraction of the remnant field

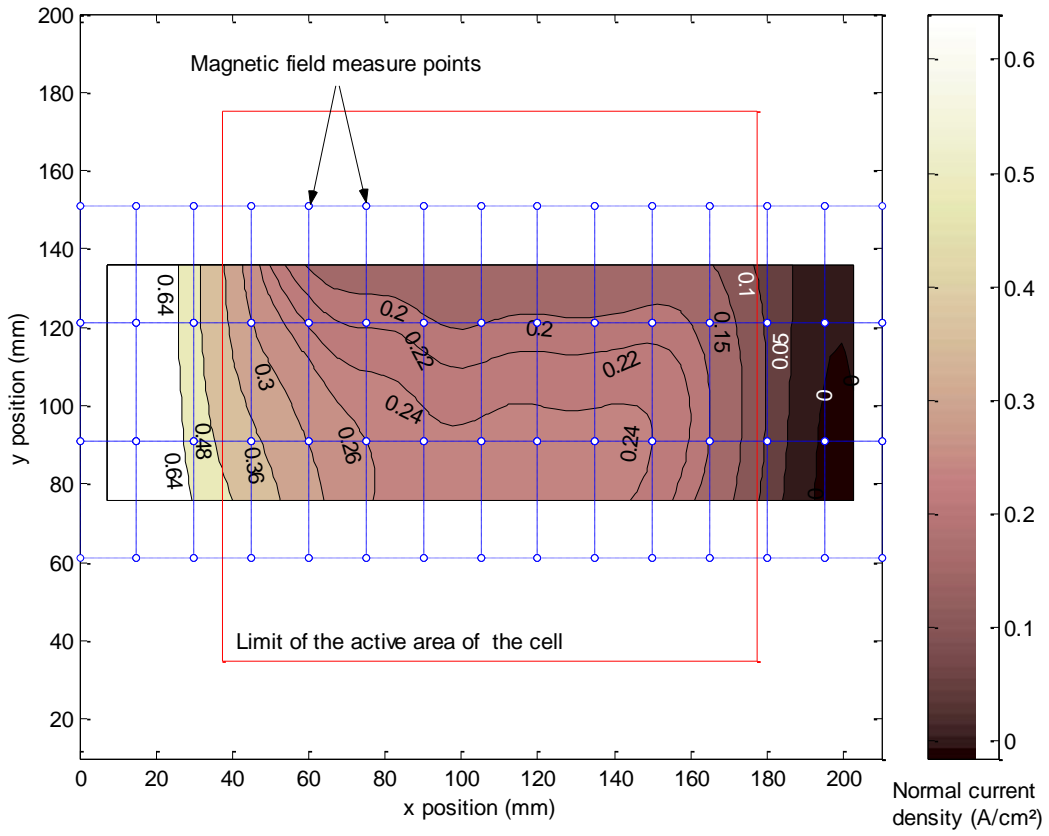


Fig. 9. Current density distribution over the cell operating at 200A.

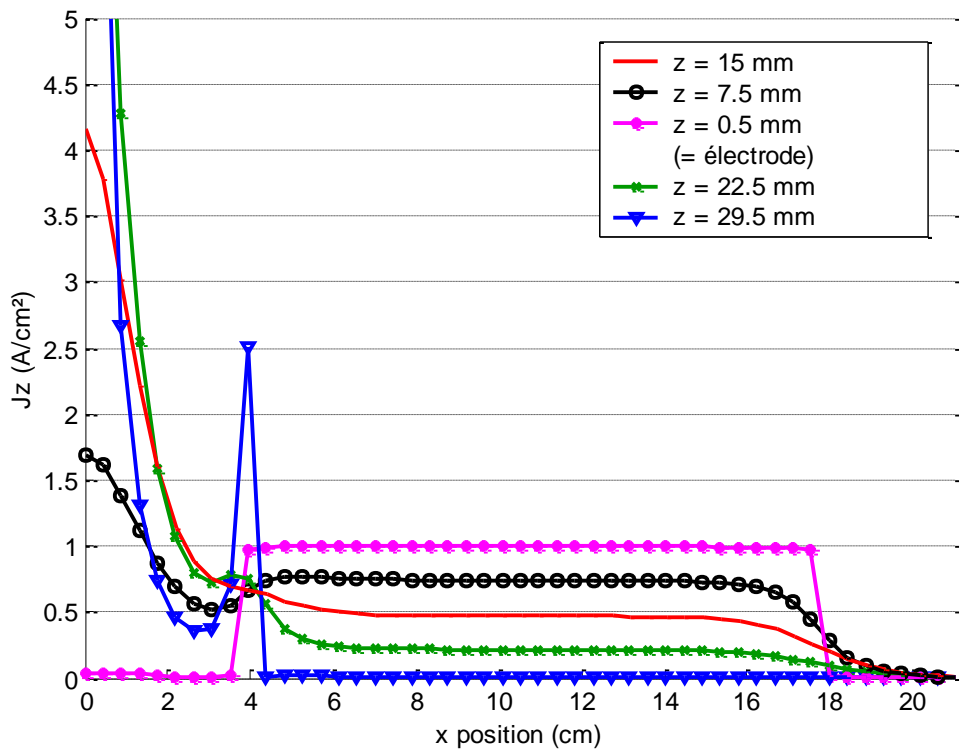


Fig. 10. J_z current density versus x position for different z .

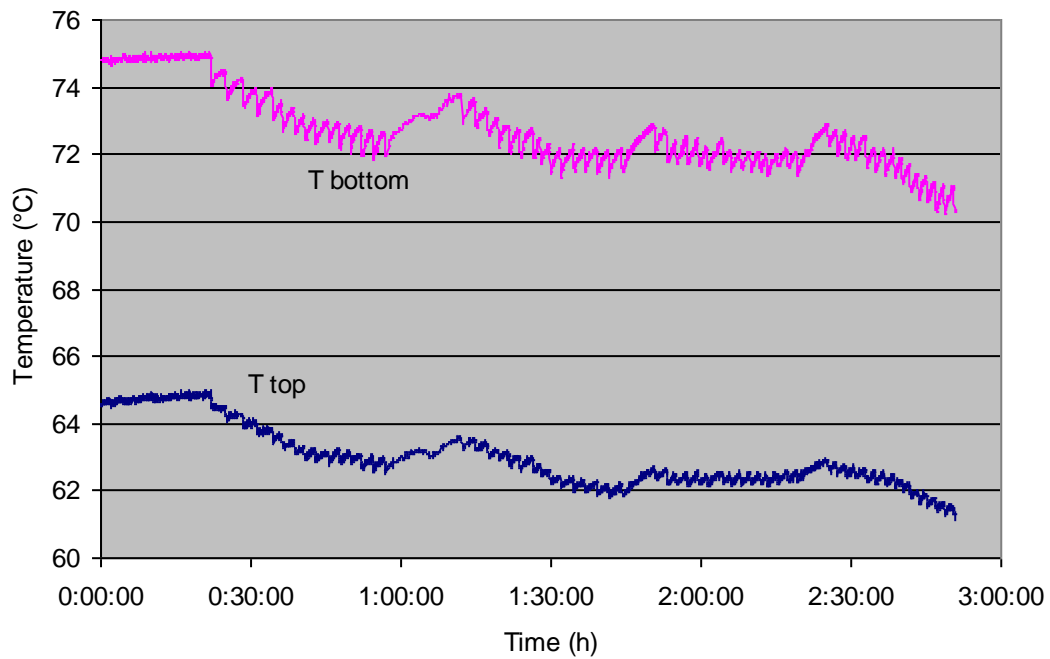


Fig. 11. Temperature measurements at the top and the bottom of the cell.

...

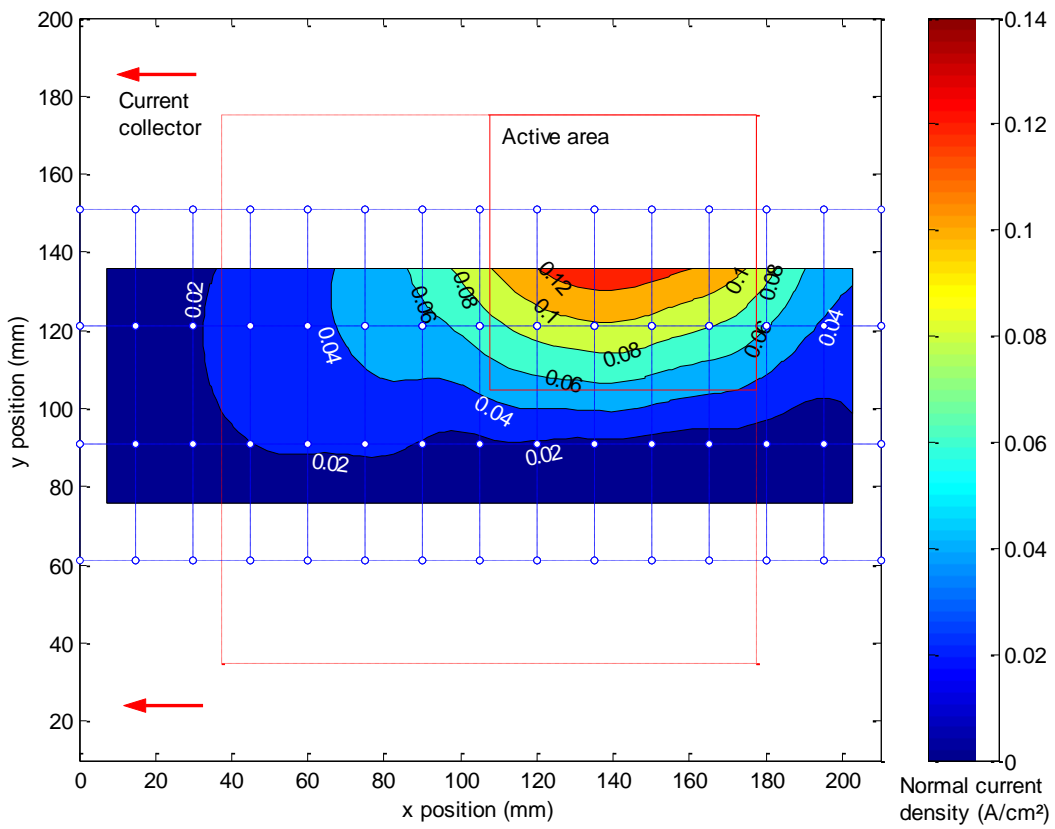


Fig. 12. Current density distribution over the cell operating at 50A (experimental results) – active area at the top of the cell, on the opposite side to the current collector plugs.

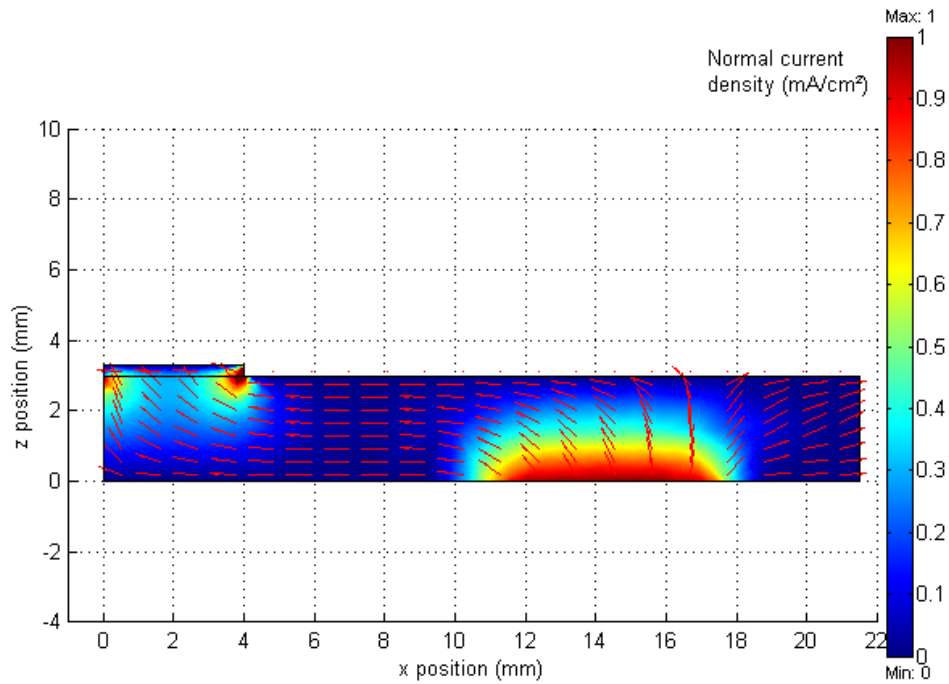


Fig. 13. Current density distribution (arrows length **not** proportional to current densities) – simulation results.

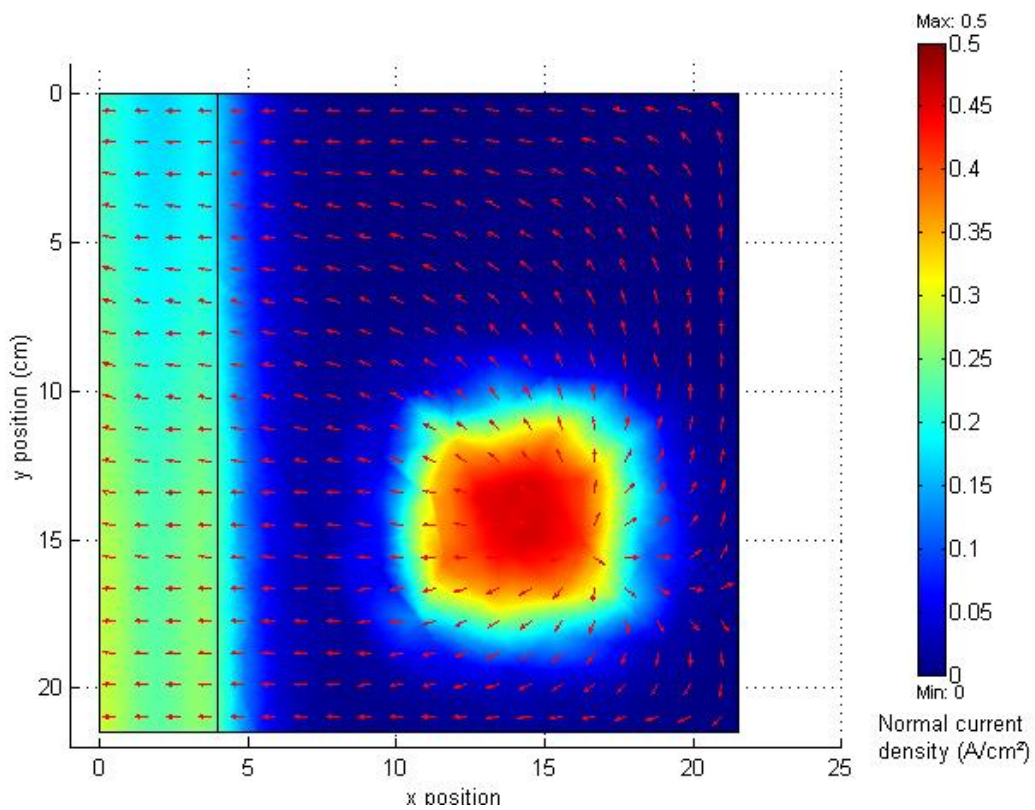


Fig. 14. Current density distribution at $z=15$ mm (arrows length **not** proportional to current densities) – simulation results.

